JACS
JOURNAL OF THE AMERICAN CHEMICAL SOCIETY
Article
pubs.acs.org/JACS

The Role of Ligands on the Equilibria Between Functional States of a G Protein-Coupled Receptor

Tae Hun Kim,[†] Ka Young Chung,[‡,§] Aashish Manglik,[‡] Alexandar L. Hansen,[∥] Ron O. Dror,[⊥] Thomas J. Mildorf,[⊥] David E. Shaw,[⊥,#] Brian K. Kobilka,[‡] and R. Scott Prosser*[,†]

[†]Department of Chemistry, University of Toronto, UTM, 3359 Mississauga Road North, Mississauga, Ontario, Canada L5L 1C6
[‡]Department of Molecular and Cellular Physiology, Stanford University School of Medicine, Stanford, California 94305, United States
[§]School of Pharmacy, Sungkyunkwan University, Suwon 440-746, South Korea
[∥]Department of Medical Genetics and Microbiology, University of Toronto, Toronto, Ontario, Canada M5S 1A8
[⊥]D. E. Shaw Research, New York, New York 10036, United States
[#]Center for Computational Biology and Bioinformatics, Columbia University, New York, New York 10032, United States

Supporting Information

ABSTRACT: G protein-coupled receptors exhibit a wide variety of signaling behaviors in response to different ligands. When a small label was incorporated on the cytosolic interface of transmembrane helix 6 (Cys-265), ^{19}F NMR spectra of the β_2 adrenergic receptor (β_2AR) reconstituted in maltose/neopentyl glycol detergent micelles revealed two distinct inactive states, an activation intermediate state en route to activation, and, in the presence of a G protein mimic, a predominant active state. Analysis of the spectra as a function of temperature revealed that for all ligands, the activation intermediate is entropically favored and enthalpically disfavored. β_2AR enthalpy changes toward activation are notably lower than those observed with rhodopsin, a likely consequence of basal activity and the fact that the ionic lock and other interactions stabilizing the inactive state of β_2AR are weaker. Positive entropy changes toward activation likely reflect greater mobility (configurational entropy) in the cytoplasmic domain, as confirmed through an order parameter analysis. Ligands greatly influence the overall changes in enthalpy and entropy of the system and the corresponding changes in population and amplitude of motion of given states, suggesting a complex landscape of states and substates.

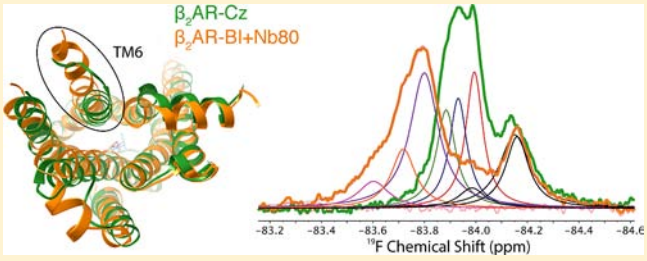

INTRODUCTION

In eukaryotes, signal transduction across the cell membrane is routinely achieved through G protein-coupled receptors (GPCRs), which respond to light or a variety of ligands, including hormones, lipids, and neurotransmitters.[1−5] Their activation by either light or ligand binding then initiates an interaction with a specific intracellular guanine nucleotide binding protein (G protein), leading to release and activation of the α subunit and downstream activation of specific signaling pathways. While most GPCRs have a similar topology, consisting of seven transmembrane α-helical segments separated by intra- and extracellular loops,[6] there is an enormous variation in ligand-dependent signaling behavior among the nearly 800 human GPCRs.

The classic view of the mechanism of action of GPCRs is that ligand binding to the extracellular pocket induces a local perturbation that triggers a conformational change on the intracellular side associated with the G protein binding interface. Computational and experimental studies have suggested that this picture is oversimplified and that, in the case of ligand-activated GPCRs, the active state is thermally accessible, though generally weakly populated without the addition of agonist.[7,8] Computational studies describe the GPCR in terms of a loosely coupled allosteric network in which distinct regions of the protein may switch between conformations consistent with inactive and active states.[9] Ligands play a key role in stabilizing or destabilizing intermediates involved in activation. For example, upon binding to an agonist, a GPCR conformer is then stabilized for a sufficient period of time to engage a G protein.[10] This picture is reminiscent of the recent NMR-based perspective, which purports that many enzymes are inherently plastic and that conformations associated with activation intermediates are frequently sampled. In this case, the role of the substrate is to alter the stabilities of key on-pathway intermediates.[11] While the entirety of ligand-dependent activation pathways is admittedly complex, it is insightful to identify key activation intermediates and the associated changes in amplitudes and time scales of domain-specific motions upon addition of ligand. Alternatively, a thermodynamic approach may be taken in an attempt to understand the role of ligands in activation. For example, a

Received: March 4, 2013
Published: May 31, 2013

   dx.doi.org/10.1021/ja404305k | J. Am. Chem. Soc. 2013, 135, 9465−9474

positive enthalpy change upon activation often reflects the loss of stabilizing interactions associated with the inactive state, while entropy gains can be associated with increased protein dynamics or the release of waters of hydration.

In this work on the human β_2 adrenergic receptor (β_2AR), we employed ^{19}F NMR spectroscopy to examine the functional states associated with the GPCR reconstituted in maltose/neopentyl glycol (MNG-3) detergent micelles. By quantifying the relative fraction of each state as a function of temperature, we were able to map out the thermodynamic equilibria between inactive states, an activation intermediate state, and active states. A van't Hoff analysis of these equilibria provided enthalpy and entropy differences between states, which were further evaluated in the presence of various ligands and a G protein mimic, termed nanobody 80 (Nb80).[12,13] Finally, an analysis of ^{19}F NMR spin relaxation rates provided a molecular perspective of both the amplitude and time scale associated with local motions in the cytoplasmic domain known to interact with the G protein.[14,15] We discuss these results in terms of our current understanding of the mechanism of action of GPCRs and the role of ligands in the process.

RESULTS

In the absence of a G protein or G protein mimic, ^{19}F NMR spectra associated with Cys-265 may be attributed to three states. To delineate functionally distinct states, we employed a trifluoromethyl tag ($-COCF_3$) located on Cys-265, near the cytosolic water interface of transmembrane helix 6 (TM6). Crystal structures of the inactive and active forms of β_2AR revealed that TM6 is displaced outward from the helical bundle upon activation, causing Cys-265 to become more solvent-exposed in the active state, as shown in Figure 1a.[16] Since ^{19}F NMR chemical shifts are sensitive to electrostatic environments and van der Waals contacts,[17] Cys-265 is an ideal labeling site to distinguish conformers related to activation. Indeed, Cys-265 has been used previously in fluorescence spectroscopy[18] and ^{19}F NMR studies[19,20] to monitor receptor activation.[21] The ^{19}F NMR spectrum of the apo form of β_2AR is shown in Figure 1b. This spectrum can be deconvolved into three components (designated S_1, S_2, and S_3) that we attribute to Cys-265 and a fourth component (designated as Δ) arising from an additional cysteine residue. We note that all of the spectra presented in this article (see Supplementary Figure S1 in the Supporting Information) were obtained from β_2AR reconstituted in MNG-3 detergent micelles, which in our hands gave rise to greater chemical shift dispersion and greater sample stability than that in *n*-dodecyl-β-D-maltoside (DDM).[20]

An alternative deconvolution of the apo β_2AR spectrum into two states, $S_{1,2}$ and S_3, is provided in Supplementary Figure S2, where the residual error in the fit is shown to be greater than the noise. Our choice to assign three states to the protein was partly based on the observation that the fitted line widths of S_1, S_2, and S_3 correspond well to the line widths estimated from T_2 relaxation measurements. In contrast, the line width of $S_{1,2}$ resulting from the assumption of two states is significantly greater than that estimated by T_2 measurements, suggesting that $S_{1,2}$ would be better represented by two or more peaks, as discussed at length in Supplementary Figures S3 and S4 and Supplementary Table T1. On the basis of T_2 measurements, which essentially permitted us to evaluate the line widths of states independently of the deconvolution, this assumption of three states held true for all of the ligands investigated.

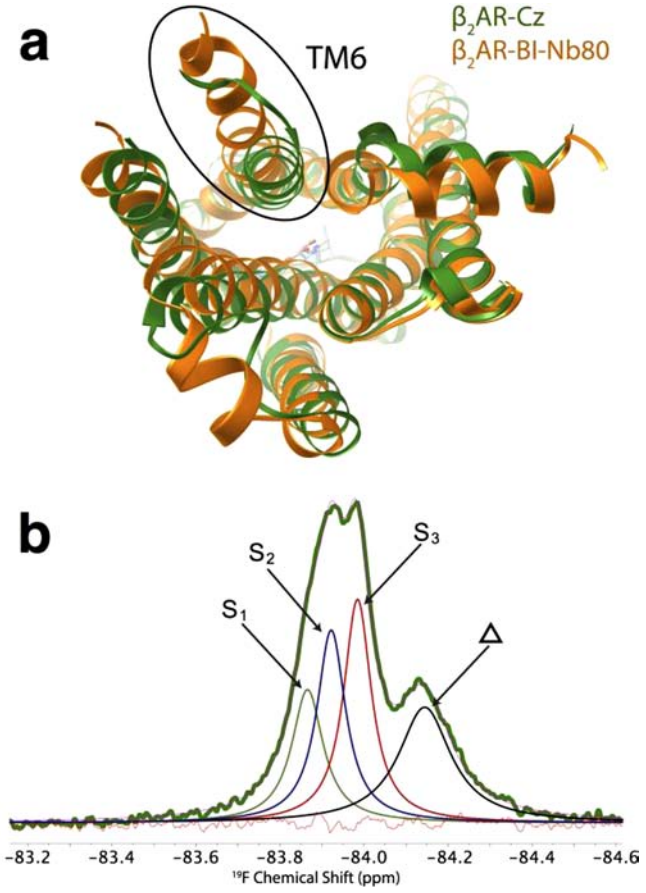

Figure 1. (a) Superimposed crystal structures of Cz-bound β_2AR (green) and BI-bound β_2AR with Nb80 (orange). The largest difference is at the end of TM6. (b) ^{19}F NMR spectrum of the apo form of β_2AR labeled with a trifluoromethyl tag at 30 °C and its spectral deconvolution, which identified three distinct functional states of the receptor (S_1, S_2, and S_3). This spectrum was published previously[20] but is shown here to introduce the states S_1–S_3. An additional peak (Δ) designates a second partially labeled cysteine residue that is not affected by ligands. The faint orange line shows the residual error associated with the fit.

The Relative Populations of the Three States Depend on the Ligand. Remarkably, the addition of saturating amounts of the inverse agonist carazolol (Cz), the partial agonist salmeterol (Salm), or the agonist BI-167107 (BI) afforded spectra that could be characterized by the same three states as defined in Figure 1b. These spectra and their deconvolutions are shown in a recently published article[20] and in Supplementary Figure S1. The principal effect of the ligand is to alter the populations of states S_1, S_2, and S_3. The absence of gross differences in line width or frequency suggests that S_1, S_2, and S_3 are in slow exchange on the NMR time scale (i.e., <150 s^{-1}). However, in view of the small differences in the chemical shifts of these states,[22−24] it was difficult to study details of the exchange dynamics via saturation-transfer or Carr–Purcell–Meiboom–Gill (CPMG) relaxation experiments, which ideally rely upon a sizable chemical shift difference between states. A second weak peak, denoted as Δ, appeared near −84.15 ppm in all of the spectra. The integral associated with Δ was unchanged by ligand, and thus, this peak likely arises from another labeled cysteine residue that is not sensitive to conformational changes (vide infra).

dx.doi.org/10.1021/ja404305k | J. Am. Chem. Soc. 2013, 135, 9465−9474

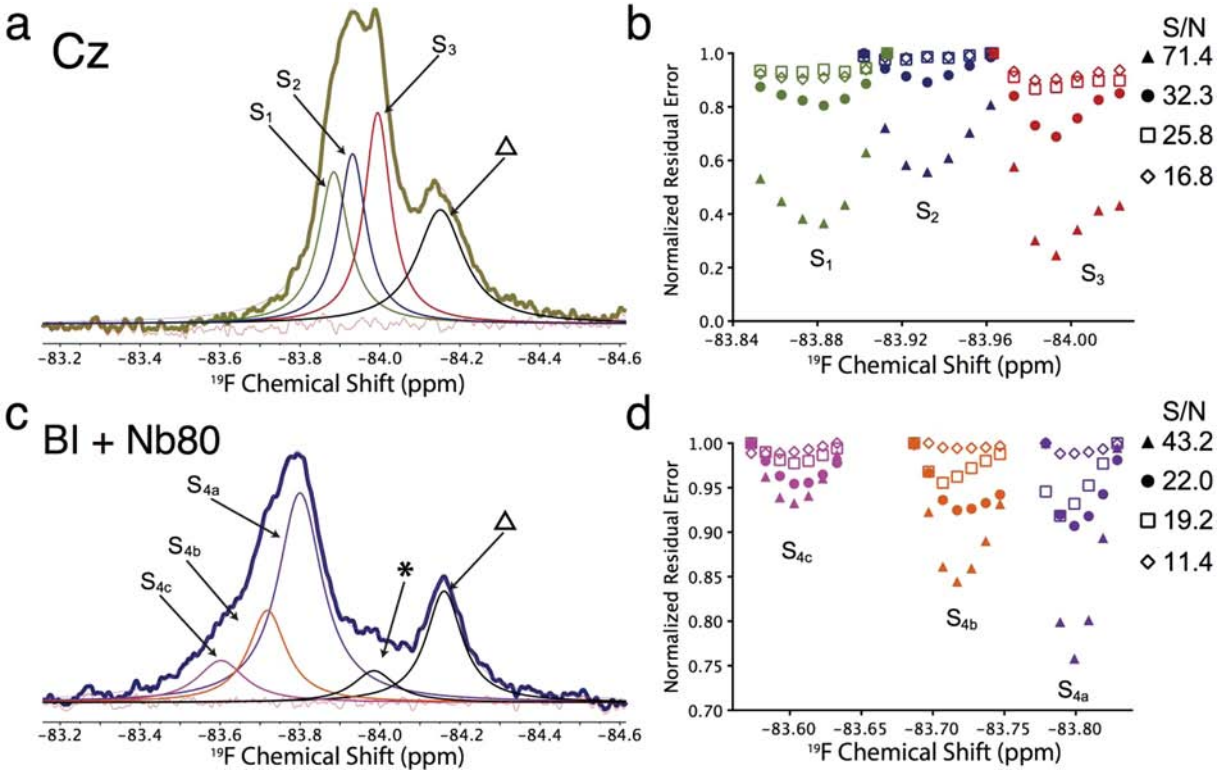

Figure 2. (a, c) Deconvolutions of ^{19}F NMR spectra of β_2AR in the presence of saturating amounts of (a) the inverse agonist Cz or (c) the agonist BI plus nanobody Nb80. These spectra were published recently[20] but are recapitulated here to assess the robustness of the deconvolution fitting parameters. (b) Error analysis of the deconvolution in (a), where the effect of the chemical shift offset on the global RMSD fitting error was separately explored for states S_1, S_2, and S_3 defined by the deconvolution. The RMSD error was normalized by dividing the error resulting from a given offset by that obtained for the greatest offset. (d) Error analysis for the spectrum of β_2AR with nanobody shown in (c). The error analyses in (b) and (d) were repeated as functions of the overall signal-to-noise (S/N) ratio resulting from the addition of noise to the spectra. The results show that with the given S/N ratio, states S_1, S_2, and S_3 can be robustly defined, while it is not possible to ascribe confidently three distinct conformers to the nanobody-stabilized spectrum.

Spectral deconvolutions such as those provided above require high-fidelity spectra with very good signal-to-noise (S/N) ratios. This is further explained in Figure 2, where the ^{19}F NMR spectra of GPCR stabilized by the inverse agonist Cz (Figure 2a) or the agonist BI plus nanobody Nb80 (Figure 2c) are shown. Upon identification of the best-fit frequencies and widths of states S_1, S_2, and S_3 in Figure 2a, a range of offset frequencies were applied to the peak associated with state S_1, whereupon a global deconvolution allowing all of the other parameters to vary was attempted. The resulting root-mean-square deviation (RMSD) for each fit was then normalized by dividing by the RMSD obtained for the greatest chemical shift offset for S_1 (green triangles in Figure 2b). This exercise was then repeated for states S_2 and S_3 (blue and red triangles, respectively, in Figure 2b). The results show that the RMSD fitting error in the global deconvolution more than doubled when an offset of ±0.04 ppm was attempted for any peak, suggesting that all three states S_1, S_2, and S_3 are robustly defined. It should be noted that the addition of noise to these spectra quickly changed the outcome, as shown in Figure 2b and Supplementary Figure S5. When the S/N ratio was reduced by more than a factor of 2, the deep fitting minima disappeared, and it was difficult to define three distinct frequencies and hence three distinct states. Figure 2d shows a similar analysis for the ^{19}F NMR spectrum of β_2AR stabilized by the agonist BI plus the G protein mimic, Nb80. In this case, the RMSD error resulting from offsetting either S_{4a}, S_{4b}, or S_{4c}, did not change as precipitously as that shown in Figure 2b. We conclude that the nanobody spectrum is characterized by a prominent single (fully active) state, S_{4a}, with the possibility of additional minor conformers characterized by shifts that are further downfield.

The results of the spectral deconvolutions as functions of ligand and nanobody are shown in Figure 3 and Supplementary

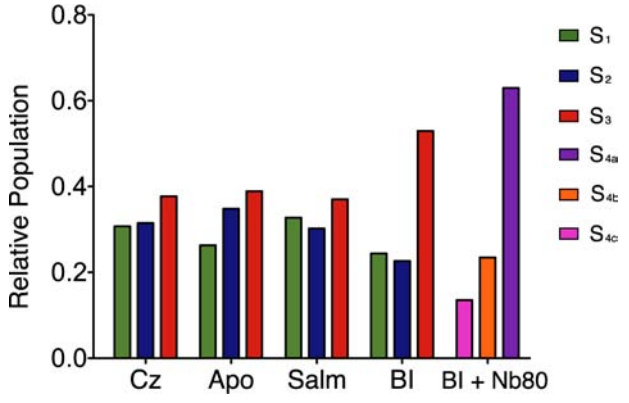

Figure 3. Relative populations of the inactive states S_1 (green) and S_2 (blue), the activation intermediate state S_3 (red), and the active states S_{4a} (purple), S_{4b} (orange), and S_{4c} (magenta) as functions of ligand. Cz, Salm, and BI designate the inverse agonist carazolol, the partial agonist salmeterol, and the full agonist BI-167107, respectively. Nb80 designates a nanobody meant to mimic the stimulatory G protein.

dx.doi.org/10.1021/ja404305k | J. Am. Chem. Soc. 2013, 135, 9465−9474

Figure S6, where the relative populations of S_1, S_2, and S_3 are expressed as functions of the ligand using the areas of the deconvolved peaks. On the basis of the effects of the inverse agonist and the agonist on the relative populations of S_1, S_2, and S_3, we assign S_1 and S_2 to distinct inactive-state conformers and S_3 to an intermediate associated with activation of β_2AR. The addition of the agonist increased the fraction of the S_3 state, which also appears most upfield. The active conformation of β_2AR is characterized by an outward shift of the intracellular end of TM6, which is consistent with the more upfield chemical shift of the activation intermediate S_3, since greater solvent exposure typically results in upfield shifts of ^{19}F NMR resonances.[17] Clearly, the nanobody has the effect of stabilizing a single (active) state, with the possibility of two minor conformers as discussed above.

The Functional States Can Be Described in Terms of Local Orientational Order and Dynamics. While the spectral deconvolutions and T_2-based line width analyses confirmed the existence of distinct inactive, intermediate, and fully active states associated with the G protein binding domain, we also could delineate these states further in terms of local reorientational dynamics. We began by assuming that the dynamics of the fluorinated reporter could be described in terms of a tumbling time (τ_M) associated with the detergent-solubilized GPCR and a correlation time (τ_e) associated with the much faster reorientations of the trifluoromethyl group at the cytosolic interface. τ_M was estimated from experimental measurements of the hydrodynamic radius (r_H) of the detergent-solubilized GPCR, which in turn were derived from diffusion rate measurements, which monitored the aromatic (protein) signal as a function of gradient strength in a pulsed-field-gradient stimulated-echo diffusion experiment.[25] The amplitude associated with the fast local reorientations is described by an orientational order parameter S^2, where S^2 = 0 corresponds to unrestricted local reorientations and S^2 = 1 is associated with a completely rigid probe. S^2 and τ_e could be reliably ascertained by a model-free analysis of the ^{19}F NMR relaxation times T_1 and T_2 at two field strengths (in our case, ^{1}H Larmor frequencies of 600 and 500 MHz; the data are shown in Supplementary Table T2).[14,15]

The model-free analysis yielded a clear trend with regard to the orientational amplitudes associated with the probes in each of the three states S_1, S_2, and S_3, as shown in Figure 4. In all cases, the orientational order was lowest for the activation intermediate (Figure 4 and Supplementary Figure S7). At the same time, τ_e was generally largest for the activation intermediate (Supplementary Figure S7). The dominant active state, S_{4a}, exhibited flexibility comparable to that of the activation intermediate S_3. We note that our $COCF_3$ trifluoromethyl probe may exhibit residual mobility different from that seen with CH_2CF_3 and other trifluoromethyl tags.[26] For this reason, we rely on the S^2 values to describe the relative mobilities of distinct states as functions of ligand.

For All of the Ligands Considered, Activation Is Entropically Driven and Enthalpically Disfavored. To explore further the role of specific states in GPCR activation, we conducted a careful analysis of the ^{19}F NMR spectra as a function of temperature. With the deconvolved spectra, it was possible to interpret the peak areas associated with states S_i as relative populations P_i (these data are shown in Supplementary Figure S8). Their ratios P_j/P_i could then be considered equal to the equilibrium constants K_{ij} for states i and j (e.g., $K_{13} = P_3/P_1$). If it is assumed that the state-specific enthalpies are

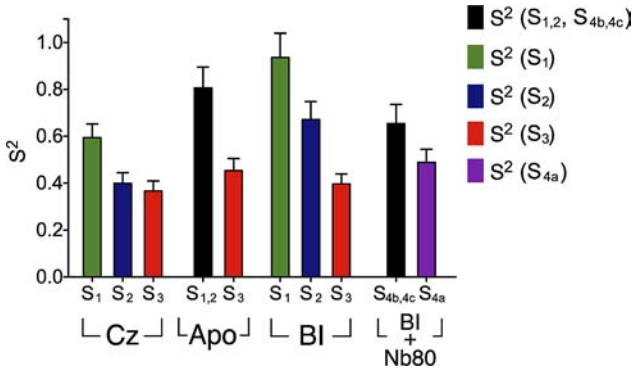

Figure 4. Experimentally derived orientational order parameters S^2 for the states S_1, S_2, and S_3 of apo β_2AR or β_2AR in the presence of either the inverse agonist Cz or the agonist BI. The orientational order parameters of the active states S_{4a}, S_{4b}, and S_{4c} resulting from addition of Nb80 to the BI-saturated sample are also included. $S_{1,2}$ designates an average of states S_1 and S_2, which could not be reliably resolved in the order parameter analysis. Similarly, $S_{4b,4c}$ represents an average of S_{4b} and S_{4c}.

constant over the temperature range investigated, the temperature dependence of the equilibrium constant K_{ij} may be expressed by the van't Hoff equation (eq 1),

$$\ln K_{ij} = -\frac{\Delta H_{ij}^{\circ}}{RT} + \frac{\Delta S_{ij}^{\circ}}{R} \quad (1)$$

where ΔH_{ij}° and ΔS_{ij}° represent the standard enthalpy and entropy differences between the states, R is the gas constant, and T is the absolute temperature. Figure 5a shows van't Hoff analyses for the inverse-agonist-saturated, apo, and agonist-saturated β_2AR samples, and the ΔH_{ij}° and ΔS_{ij}° values obtained from the van't Hoff analyses are shown in Figure 5b,c, respectively. In some cases it was possible to discriminate only two states reliably over the entire temperature range. In these cases, the equilibrium constants and corresponding thermodynamic parameters represent a state corresponding to an average of the two minor states versus the major state; the equilibria are thus reported as $K_{(1,2)3}$ or $K_{(4b,4c)4a}$.

DISCUSSION

States and Populations. A significant body of evidence suggests that GPCRs are not simple two-state switches but rather encompass a wide spectrum of states and conformations.[5,27,28] Recent spectroscopic studies have echoed the suggestion of multiple states.[20,28,29] For example, Liu et al.[19] examined the idea of biased agonism and found evidence that specific ligands favor one of two conformations, thereby selecting for distinct signaling pathways. In the current study, two inactive states, S_1 and S_2, account for roughly 60% of the total spectral intensity for the apo and inverse-agonist-saturated β_2AR samples. Recent molecular dynamics (MD) simulations of the inactive state of β_2AR revealed an alternative inactive conformer in which the intracellular half of TM7 (Asn318–Cys327, including the conserved NPxxY motif) is rotated ~40° clockwise relative to the crystal structure (viewed from the intracellular side) and shifted toward the center of the helical bundle by ~3 Å.[9,29] This state is believed to exchange slowly with the crystallographically observed inactive state in the presence of inverse agonists or in the absence of a ligand.[29] Thus, it seems likely that S_1 and S_2 represent two distinct inactive-state conformers. Interestingly, the partial agonist

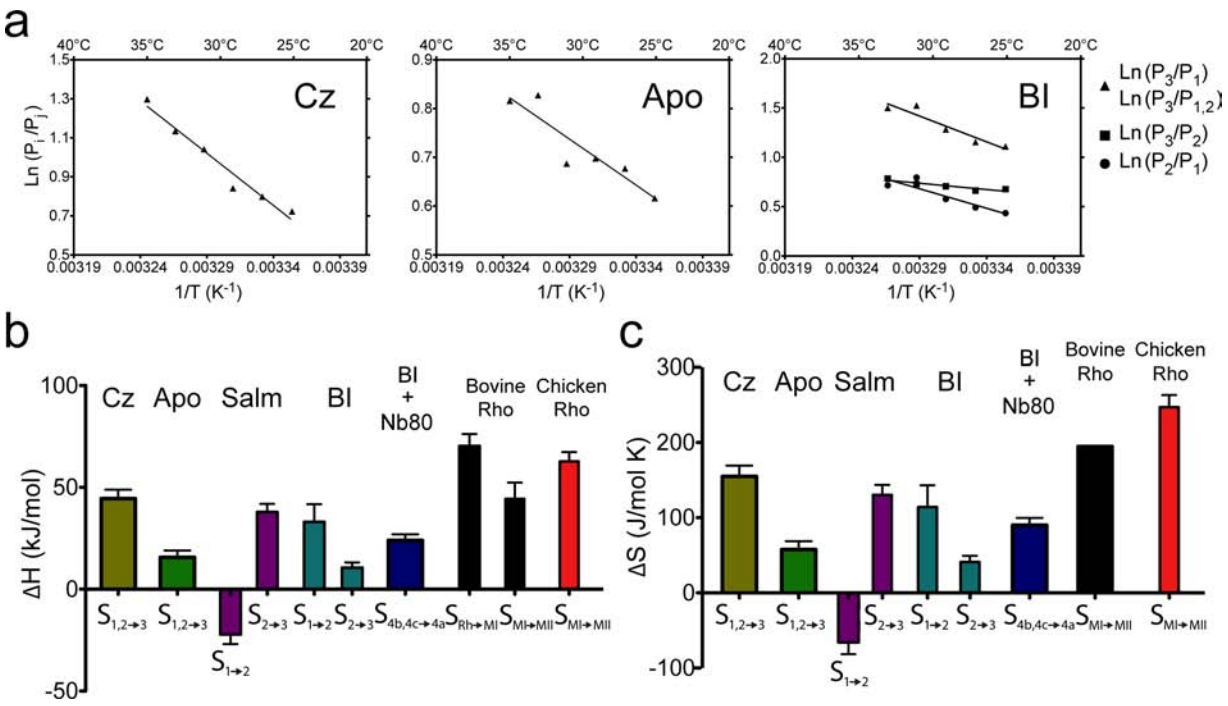

Figure 5. (a) Van't Hoff analyses of (left, center) the equilibrium constant $K_{(1,2)3}$ for (left) apo β_2AR and (center) β_2AR treated with the inverse agonist Cz and (right) the equilibrium constants K_{13}, K_{23}, and K_{21} associated with β_2AR in the presence of the agonist BI. (b, c) Differences in (b) enthalpy (ΔH°_{ij}) and (c) entropy (ΔS°_{ij}) between distinct functional states of β_2AR as functions of ligand. The corresponding enthalpy and entropy differences between the inactive and active states of bovine and chicken rhodopsin (Rho) are provided for comparison.

(Salm) seemed to favor the S_1 state, as shown in Figure 3. The addition of agonist (BI) similarly favored S_1 over S_2, although by far the greatest effect of the agonist is to stabilize the S_3 state.

A recent NMR study of β_2AR also identified two distinct inactive states and an agonist-activated state.[28] Here, the two inactive states were comparably populated upon addition of the inverse agonist (Cz), while addition of the agonist caused an increase in the population of S_3, which we assign as an activation intermediate. We note that the observation of three distinct states was possible only with the new detergent MNG-3.[20] Exactly how these three states relate to the observation of two states and the concept of biased agonism is unclear, since the study by Liu et al.[19] was performed using DDM micelles, which in our hands gave rise to a single motionally narrowed peak in fast exchange between two or more states.[20] It was also possible for us to delineate three states only after achieving exceptional S/N ratios for all of the spectra, as outlined in Figure 2. Moreover, we can be confident that the states S_1, S_2, and S_3 are distinct and functional since all of the samples were purified in the final step by ligand-affinity chromatography and all states responded to both ligand and the addition of nanobody.

Dror et al.[9] utilized MD simulations beginning with a G protein-stabilized active conformation[16] to identify an on-pathway intermediate state of the G protein binding domain. Both the intermediate and active conformations are distinguished by an outward shift of the intracellular end of TM6. These authors also proposed that the G protein may first bind to the GPCR in the intermediate state. Binding then promotes conversion to the active state. We conclude that S_3 represents an on-pathway intermediate toward a fully active state, which is achieved upon binding to either a G protein or a G protein mimic. This same conclusion was recently reached in an NMR study of [^{13}C]methionine-enriched β_2AR.[29] There is also some recent evidence based on radiolytic footprinting and deuterium exchange studies suggesting that rhodopsin (Rho) exhibits similar behavior in the sense that the light-activated state (Rho*) exhibits a different topology than the fully active complex with the G protein (Rho*−G_t).[30]

The addition of the G protein mimic, Nb80, is believed to stabilize the active conformation of β_2AR fully.[12] In our hands, the addition of Nb80 resulted in a completely distinct peak, denoted S_{4a} in Figure 2, with two smaller peaks, denoted S_{4b} and S_{4c}. Since Cys-265 is known to be more than 5 Å from the van der Waals surface of Nb80 on the basis of computational analysis, it is more likely that the shift arises from a conformational change to a distinct active state rather than a chemical shift perturbation due to binding of Nb80 (it should be noted that the Δ peak did not shift upon the addition of Nb80). Binding of the nanobody presumably reinforces the entire structure in such a way that it adopts a fully active state, designated as S_{4a}, while S_{4b} and S_{4c} may represent distinct minor conformers, possibly resulting from alternate modes of interaction between the receptor and the nanobody. β_2AR couples the binding of specific agonists to the activation of either the stimulatory or inhibitory heterotrimeric G proteins (G_s or G_i, respectively) while alternatively signaling through mitogen-activated protein kinase pathways in a G protein-independent manner via β-arrestin.[31] Given the signaling promiscuity of β_2AR, one can well imagine an active state or an activation intermediate whose conformation is compatible with one or more G proteins that adopts the appropriate G protein-specific conformation via a combination of presampling and induced fit. The minor states S_{4b} and S_{4c} could therefore represent alternative active states that are stabilized by interactions with G_i or β-arrestin mimics, though this remains to be shown. Alternatively, the minor states might be necessary to facilitate the process of deactivation or G protein decoupling.

dx.doi.org/10.1021/ja404305k | J. Am. Chem. Soc. 2013, 135, 9465−9474

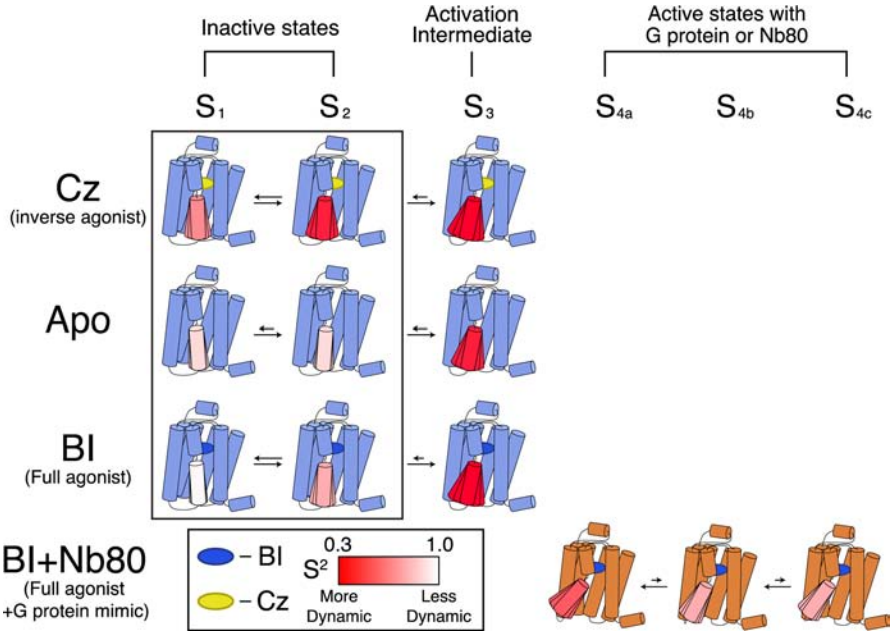

Figure 6. Schematic illustration of the ensemble of states identified by ^{19}F NMR and the effect of ligands and nanobody (Nb80) on both the conformational equilibria and disorder of the cytosolic domain. For all ligands, there is an increasing trend in local dynamics of Cys265 with degree of activation while activation intermediate states (S_3) are the most dynamic among all states. In case of one of the inactive states, S_1, the local dynamics decrease as a function of efficacy of ligand. Note that active states are only accessible with a G protein or Nb80. Low order parameters (S^2) are represented in red while high order parameters being represented in white.

While outside the current scope of this work, it is feasible that the active-state ensemble may indeed consist of a number of stable conformations.

Clearly, ligands predominantly influence the populations of a distinct ensemble of states, though there may well be accompanying changes in the lifetimes of these states. However, it is surprising that the addition of inverse agonist or partial agonist causes a relatively small change in the state populations. In a recent study examining NMR spectra of [^{13}C]methionine-enriched β_2AR, the authors identified key regions of the transmembrane domains in which two distinct inactive states could also be observed.[28,29] While their observations are similar to ours, the relative populations are quite different, and the activation intermediate was apparent only upon addition of agonist. Part of this apparent difference arises from the fact that the relative volume of a peak in a two-dimensional ^{13}C,^{1}H spectrum is not representative of the population, since the requisite insensitive nuclei enhanced by polarization transfer (INEPT) transfer periods cause significant losses in intensity of the peaks with the lowest T_2 relaxation times. In ^{19}F NMR spectroscopy, or indeed any directly detected one-dimensional NMR technique, the relative areas of the deconvolved peaks should faithfully reproduce the relative populations. A weak response to ligand through populations assessed from a single domain may be a consequence of the fact that the GPCR is a loosely coupled system. Distinct changes in the ligand binding domain give rise to probabilistic changes in the conformers associated with the connecting region and cytosolic domain of the GPCR. However, the changes in lifetimes and dynamics of states upon addition of ligand may play a key role in affecting activation. Alternatively, the weak response to ligands measured here may reflect the fact that our measurements are sensitive only to a subset of the degrees of freedom of the G protein binding domain.

Order and Dynamics. The motional amplitudes of distinct states are also greatly influenced by the ligand, as depicted in Figure 6. The activation intermediate exhibits the greatest amplitude of motion, regardless of ligand. MD simulations and crystallographic studies of agonist-saturated β_2AR tend to result in a single low-energy state consistent with the inactive conformation, so it is perhaps not surprising that the activation intermediate state exhibits the largest-amplitude short-time-scale (subnanosecond) dynamics, at least prior to binding to the G protein mimic. Higher disorder of the G protein binding region would also provide the greater conformational plasticity needed to achieve efficient coupling to the G protein if the interaction is facilitated by an induced fit mechanism.[32]

Figure 6 also illustrates the idea that orientational order is also greatly influenced by the ligand. In particular, the addition of agonist results in overall greater rigidity of the S_1 and S_2 states in comparison with that observed with inverse agonist, while the orientational order of the activation intermediate does not change with ligand. One can interpret the orientational order in terms of averaging of underlying short-time-scale substates: a higher order parameter represents a more restricted ensemble of substates.[10] The addition of agonist increases the relative population of the activation intermediate while at the same time restricting the ensemble of substates for S_1 and S_2. The inverse agonist has exactly the opposite effect, producing greater disorder among the inactive states and a wider spectrum of substates within S_1 and S_2. In all cases, S_3 remains the most dynamic of these states. Thus, while the ligand clearly influences the state populations, there is a pronounced effect of the ligand on the average orientational order of states, particularly the inactive states. One interpretation is that a given state represents an average over rapidly interconverting substates whose distribution and interconversion rates define the roughness of the landscape. Ligands influence the substate distribution and roughness, presumably affecting the overall

dx.doi.org/10.1021/ja404305k | J. Am. Chem. Soc. 2013, 135, 9465−9474

lifetimes and exchange rates of the states. For example, the addition of agonist causes the reorientational amplitude of the S_1 state to decrease and that of S_2 to increase in comparison with the apo state, which presumably influences the activation kinetics and pathways.

Thermodynamics of Activation. As shown in Figure 5, an analysis of the temperature dependence of the populations of the S_1, S_2, and S_3 states revealed that activation is enthalpically unfavorable and entropically favorable, regardless of the ligand. We emphasize that these results pertain to the GPCR + water system as a whole, despite the fact that the spectroscopic reporter is confined to a single residue on the protein. Enthalpy and entropy differences associated with activation from rhodopsin to a meta I intermediate (MI) and from MI to the meta II active state (MII) based upon values reported in the literature[5,33] are also shown in Figure 5. While rhodopsin activation is also enthalpically unfavorable and entropically favorable, the magnitudes of the activation steps are smaller in the case of β_2AR for all of the ligands investigated. The differences in enthalpy likely relate to the fact that β_2AR exhibits basal activity whereas rhodopsin requires strict control; the active state is only attained once retinal has undergone light-induced cis−trans isomerization.[34,35] The rhodopsin inactive state is partly stabilized through a so-called ionic lock, which holds together helices 3 and 6 and serves as a molecular switch.[18,34,35] In other words, the rhodopsin inactive state is considerably more stable and requires a greater net input of energy for activation. In contrast, recent MD simulations and X-ray crystallographic studies of β_2AR revealed that the inactive state exists as an equilibrium between a state in which the ionic lock is engaged and one where it is released.[36,37] Thus, the enthalpy changes required for activation are smaller for β_2AR than for rhodopsin. As shown in Figure 5, there is a very clear trend with regard to the enthalpy change toward activation of β_2AR as a function of ligand. Enthalpy changes toward activation are greatest for Cz-bound β_2AR, likely reflecting the additional stability conferred to the inactive state in the vicinity of the binding pocket. In the agonist-bound state, the enthalpy changes are smallest, reflecting the underlying destabilizing effect of the agonist on the inactive state. Finally, the partial agonist also exerts a dramatic influence on the enthalpy differences between states S_1, S_2, and S_3, although activation to S_3 is clearly enthalpically unfavorable and entropically favored.

Despite the close similarity of the spectra of apo and inverse-agonist-bound β_2AR (Figure 2), there is a striking difference between the observed enthalpy and entropy changes upon activation. Unliganded β_2AR, which is known to exhibit significant basal activity, exhibits markedly lower enthalpy and entropy differences between the inactive and active intermediate states than inverse-agonist-bound β_2AR. This is consistent with the picture emerging from recent MD simulations based on X-ray crystal structures of the fully active and inactive forms, where the GPCR is described as inherently flexible and loosely coupled.[9] This "loose coupling" implies lower barriers toward activation and a lower enthalpic difference between the inactive and active states relative to a strongly coupled receptor such as rhodopsin.

For all of the ligands, the trend toward higher entropy upon activation is also consistent with prior observations for rhodopsin. Essentially, we envisage the β_2AR inactive state as being "stiffer" overall than the activation intermediate. Thus, conversion to the intermediate should involve an even greater increase in entropy through increased dynamics. Thus, the change in entropy in going from the inactive state to the activation intermediate is positive, though progressively smaller in magnitude for inverse-agonist-saturated, apo, and agonist-stabilized β_2AR, reflecting the relative state of "disorder" of the initial (inactive) state. A number of proteins have been recognized to exhibit lower orientational order and higher configurational entropy associated with the active-state ensemble, thereby driving activation.[38,39] If the cytosolic domain exhibits a greater amplitude of motion in the activation intermediate state, this may present a way for the protein to sample the active state more frequently. The model-free analysis discussed earlier also revealed that for all of the ligands investigated, the activation intermediate exhibits the lowest order parameter and longest correlation time (τ_e). This may be important for coupling to the G protein.[10]

An entropy increase associated with activation need not arise entirely from increased dynamics. While the order parameter analysis did indeed reveal the amplitude of motions to be greatest for S_3, the positive entropy change also likely arises from the liberation of water. Recently, a 1.8 Å crystal structure of the adenosine A_{2A} receptor revealed a strongly ordered water network in the inactive state.[40] Others have emphasized the importance of conserved waters in the activation process.[30,41,42] The extension of TM6 upon activation would likely disturb this network, thereby releasing ordered waters at the cytoplasmic interface. This process would also contribute to the overall positive entropy change associated with activation while facilitating binding to the G protein or other effector molecules.

■ CONCLUSIONS

β_2AR, like many GPCRs, is a remarkably versatile signaling molecule whose activation is exquisitely sensitive to the binding ligand. Using a $COCF_3$ tag on TM6 in the vicinity of the G protein binding domain, we found evidence for three states in the absence of nanobody or G protein. We assign these three states to two distinct inactive states and an activation intermediate. The addition of a ligand, either an inverse agonist, a partial agonist, or a full agonist, changes the relative populations of these states. The fully active state, which we presume to be represented by S_{4a}, is attainable only through the addition of a G protein mimic. Two other minor peaks result from the addition of nanobody, though their roles remain uncertain. It is likely that the S_{4a} state represents that crystallized with Nb80[12] and is highly similar to the receptor conformation seen in the crystal structure of the β_2AR−G_s complex.[16] As such, S_{4a} likely represents the G protein-coupled conformation of the receptor and is fully competent to signal. It is difficult to speculate about the signaling output of the activation intermediate S_3. Because the agonist BI increases the proportion of this conformation, it is likely that the intermediate is a conformation associated with G protein recruitment and subsequent signaling. However, it is not possible to determine whether the conformation of the activation intermediate is capable of binding to G protein and inducing nucleotide exchange.

The amplitudes and frequencies of local motions associated with the cytosolic domain were also assessed through T_1 and T_2 spin-relaxation experiments. The activation intermediate was observed to exhibit the greatest amplitude of motion in the apo state or in the presence of any ligand. Ligands have a profound effect on the amplitudes and frequencies, as shown in Figure 6. A thorough analysis of the thermal equilibria between these

dx.doi.org/10.1021/ja404305k | J. Am. Chem. Soc. 2013, 135, 9465−9474

states revealed that activation is enthalpically disfavored and entropically favored, as has been observed in rhodopsin. Even in the presence of an inverse agonist, which stabilizes the inactive state, the enthalpy changes are still not as great as those observed in rhodopsin, reinforcing the picture of β_2AR as a much more dynamic GPCR than rhodopsin, at least in the inactive state. Activation is clearly entropically driven. The positive entropy changes accompanying activation are likely a result of greater motional amplitudes and consequently greater configurational entropy in the activation intermediate, as evidenced by the changes in the order parameter in the cytosolic domain. Water too may play a significant role in activation in that water molecules are released into the bulk phase upon activation, thereby contributing to the overall gain in entropy of the system.[9]

The magnitudes of the enthalpy and entropy changes are generally lower for β_2AR than for rhodopsin, a likely consequence of basal activity associated with β_2AR. Moreover, while the spectra and relative populations of the inactive and activation intermediate states were observed to be very similar in the case of apo and inverse-agonist-bound β_2AR, the magnitudes of the enthalpy and entropy changes associated with activation of the apo state are much lower. This is coincident with the greater constitutive activity of the apo state and speaks to the notion of protein plasticity. Future experiments focusing on exchange between functional states should prove insightful toward understanding the influence of ligands on the energy barriers between states.

EXPERIMENTAL SECTION

β_2AR-Δ4 Generation, Purification, and Labeling with Bromotrifluoroacetone. As previously described,[43] we utilized a minimal cysteine version of β_2AR with the following mutations: C77V, C275S, C378A, and C406A. To facilitate purification of the receptor, an M1 Flag affinity sequence was appended to the N-terminus and six histidines were appended to the C-terminus. The β_2AR-Δ4 construct was expressed in Sf9 insect cells using baculovirus derived from the pFastBac system (Invitrogen). Insect cell cultures were grown in the presence of 1 μM alprenolol to increase the protein yield.

Cell pellets were lysed by osmotic shock, and the membrane fraction was isolated by centrifugation. Membranes containing β_2AR-Δ4 were solubilized in a buffer composed of 20 mM HEPES (pH 7.5), 100 mM NaCl, 1% DDM, 0.01% cholesterol hemisuccinate, and 1 μM alprenolol. The solubilized fraction of β_2AR-Δ4 was purified by M1 Flag affinity chromatography to yield biochemically pure receptor. To label the receptor, 50 μM tris(2-carboxyethyl)phosphine (TCEP) was first added to reduce any cross-linked receptor, and 100 μM 3-bromo-1,1,1-trifluoroacetone (BTFA) then added. The labeling reaction was incubated on ice for 1 h and quenched with 2 mM cysteine. Further purification of functional labeled β_2AR-Δ4 receptor was achieved by alprenolol/sepharose chromatography followed by an M1 Flag chromatography step to concentrate the receptor and exchange the detergent from DDM to MNG-3. Detergent exchange was performed over the course of 3 h during which the DDM detergent was gradually replaced with 0.01% MNG-3. To remove alprenolol fully and produce homogeneously unliganded receptor, the M1 Flag resin was washed for 1 h in 0.01% MNG-3 buffer supplemented with the low-affinity, fast-kinetics antagonist atenolol at a concentration of 30 μM. This step was followed by a 30 min wash with 0.01% MNG-3 buffer containing no ligand to achieve full displacement of bound alprenolol. Functional β_2AR-Δ4 in MNG-3 micelles was eluted in 0.01% MNG-3 buffer supplemented with 1 mM EDTA and 0.2 mg/mL Flag peptide. To ensure full labeling of β_2AR-Δ4, a 4-fold molar excess of BTFA was again added to the receptor, and the mixture was incubated at 4 °C overnight. Excess BTFA was removed by overnight dialysis in a buffer composed of 20 mM HEPES (pH 7.5), 100 mM NaCl, and 0.01% MNG-3. All of the GPCR samples were confirmed to be in monomeric form.[44] Finally, the sample was concentrated to 60 μM using a spin concentrator with a molecular-weight cutoff of 50 kDa (GE Healthcare). Ligands and Nb80 were added at a saturating concentration of 150 μM and incubated with β_2AR for >24 h before spectra were acquired. Nb80 was expressed in *Escherichia coli* and purified as described previously.[12]

As BTFA is a relatively small tag, the labeling protocol also resulted in partial labeling of two additional less-exposed cysteine residues, as evidenced by the ^{19}F NMR spectra upon digestion with protease K (Supplementary Figure S9). The total area of the two minor peaks in Figure S9 is roughly 30%. Coincidentally, a peak (labeled Δ) was identified in the β_2AR spectra that did not respond to ligand or nanobody and represented 27% of the total spectral area. Thus, this peak is presumed to arise from a separate cysteine. A second very minor peak (labeled as * in Figure 2c) is believed to arise from another partially labeled residue. The sum of the areas from the * and Δ peaks was observed to be 30% of the total spectral intensity and found to be independent of ligand and nanobody.

NMR Spectroscopy. Most of the NMR experiments were performed on a 600 MHz Varian Inova spectrometer using a cryogenic probe capable of ^{19}F NMR spectroscopy. A limited number of relaxation measurements were also performed on a 500 MHz Varian Unity spectrometer equipped with an ^{19}F room-temperature probe. Typical spectra were acquired with 8192 scans, a repetition time of 1 s, a $^{\pi}/_{2}$ pulse length of 14.5 μs, and an acquisition time of 0.25 s. Spectra were processed with MestReNova software. Free induction decay (FID) signals consisting of 14k complex points in the direct dimension were typically linear-predicted for the first 2−4 points in the FID and then zero-filled to 32k points and apodized with a Lorentzian filter equivalent to 4 Hz broadening.

T_1 was obtained using an inversion recovery sequence wherein every second scan involved a simple excitation pulse. In the difference spectrum, the spectral intensity decayed exponentially with an interpulse separation τ. Generally eight or nine τ values were used to fit each deconvolved peak to an exponential decay, with a time constant T_1. T_2 was similarly obtained via a CPMG sequence in which the total evolution time was augmented for a fixed refocusing frequency. Using eight or nine sampling times, the exponential decay in spectral intensity with time could be fitted to determine the relaxation rate $R_2 = 1/T_2$.

Our choice of three states in the deconvolutions was based on the following observations: (1) A deconvolution consisting of two states produced a fit with residual errors that were well above the noise (Figure 2). (2) The addition of a variety of ligands resulted in spectra that upon deconvolution independently yielded the same three resonances and similar line widths, with the principal difference lying in the relative intensities. Overall, it was necessary to employ three states to describe the effect of all of the ligands examined. (3) The line widths derived from a deconvolution into three resonances corresponded roughly to the measured T_2 relaxation times. A similar analysis using the assumption of two states resulted in a gross

discrepancy between the line widths derived from T_2 data and the much broader lines derived from the deconvolution. More importantly, the line width of the downfield peak $S_{1,2}$ resulting from the assumption of two states was significantly greater than that estimated by T_2 measurements. This shows that $S_{1,2}$ was best represented by two or more peaks.

An evaluation of the error associated with the deconvolution into three states was performed by first examining for each peak the effect of an offset on the global fit, as discussed in the text. The robustness of the fit was also considered as noise was folded into the spectra. Noise spectra were recorded on the spectrometer using identical conditions without sample. These noise spectra were then added to the experimental spectra to achieve the desired S/N ratios. The analysis revealed that high S/N ratios were needed to achieve a reliable deconvolution into three states for all of the ligand samples.

In assessing equilibria between states as a function of temperature, several temperature points were repeated to ensure that there were no significant hysteresis effects. At the same time, each temperature analysis required roughly 3 days of NMR time, which placed constraints on sample stability. In general, measurements at temperatures of 30 °C or more resulted in changes in the spectra after 7−10 days.

T_1 and T_2 data obtained at two field strengths for most samples were combined with estimates of τ_M from ^{1}H diffusion measurements to estimate τ_e and S^2. The fitting uncertainities in the T_1 and T_2 data were used to generate an input set consisting of thousands of possible values, whereupon a Monte Carlo fit was performed to estimate τ_e and S^2. With Stokes Law, the rotational correlation time (τ_M), hydrodynamic radius (r_H), and viscosity were calculated from the decay of the ^{1}H aromatic protein peaks and the water peak as a function of gradient strength in a stimulated-echo NMR experiment. The r_H value for the ligand-only sample was found to be 3.5 nm with a corresponding τ_M of 93.9 ns. For the BI + Nb80 sample, r_H = 3.7 nm and τ_M = 111 ns.

■ ASSOCIATED CONTENT

Supporting Information

Deconvolutions of ^{19}F NMR spectra of β_2AR as a function of ligand assuming two inactive states (Figure S1) or a single inactive state (Figure S2); characteristic T_2 relaxation series showing deconvolutions and typical noise assuming two inactive states (Figure S3) or a single inactive state (Figure S4); comparison of spectra as a function of S/N ratio (Figure S5); relative populations of states as functions of ligand (Figure S6); values of S^2 and τ_e as functions of ligand (Figure S7); populations used in the van't Hoff analyses (Figure S8); ^{19}F NMR study after protease digestion (Figure S9); comparison of line widths extracted from deconvolutions and T_2 relaxation experiments (Table T1); and relaxation rates as functions of ligand and field strength used to calculate S^2 and τ_e values. This material is available free of charge via the Internet at http://pubs.acs.org.

■ AUTHOR INFORMATION

Corresponding Author

scott.prosser@utoronto.ca

Notes

The authors declare no competing financial interest.

■ ACKNOWLEDGMENTS

R.S.P. acknowledges NSERC for a Research Discovery Award (Grant 261980). B.K.K. acknowledges funding by NIH (Grant NH028471). K.Y.C. acknowledges the National Research Foundation of Korea (NRF), funded by the Ministry of Education, Science and Technology (2012R1A1A1039220). We are also grateful to Professor Oliver P. Ernst (University of Toronto) and Dr. Adriaan Bax (NIH) for helpful discussions.

■ REFERENCES

(1) Christopoulos, A.; Kenakin, T. *Pharmacol. Rev.* **2002**, *54*, 323−374.
(2) Katritch, V.; Cherezov, V.; Stevens, R. C. *Trends Pharmacol. Sci.* **2012**, *33*, 17−27.
(3) Reiter, E.; Ahn, S.; Shukla, A. K.; Lefkowitz, R. J. *Annu. Rev. Pharmacol. Toxicol.* **2012**, *52*, 179−197.
(4) Shukla, A. K.; Xiao, K.; Lefkowitz, R. J. *Trends Biochem. Sci.* **2011**, *36*, 457−469.
(5) Park, P. S.-H.; Lodowski, D. T.; Palczewski, K. *Annu. Rev. Pharmacol. Toxicol.* **2008**, *48*, 107−141.
(6) Tate, C. G.; Schertler, G. F. *Curr. Opin. Struct. Biol.* **2009**, *19*, 386−395.
(7) Dror, R. O.; Pan, A. C.; Arlow, D. H.; Borhani, D. W.; Maragakis, P.; Shan, Y.; Xu, H.; Shaw, D. E. *Proc. Natl. Acad. Sci. U.S.A.* **2011**, *108*, 13118−13123.
(8) Rosenbaum, D. M.; Zhang, C.; Lyons, J. A.; Holl, R.; Aragao, D.; Arlow, D. H.; Rasmussen, S. G. F.; Choi, H.-J.; DeVree, B. T.; Sunahara, R. K.; Chae, P. S.; Gellman, S. H.; Dror, R. O.; Shaw, D. E.; Weis, W. I.; Caffrey, M.; Gmeiner, P.; Kobilka, B. K. *Nature* **2011**, *469*, 236−240.
(9) Dror, R. O.; Arlow, D. H.; Maragakis, P.; Mildorf, T. J.; Pan, A. C.; Xu, H.; Borhani, D. W.; Shaw, D. E. *Proc. Natl. Acad. Sci. U.S.A.* **2011**, *108*, 18684−18689.
(10) Deupi, X.; Kobilka, B. K. *Physiology* **2010**, *25*, 293−303.
(11) Eisenmesser, E. Z.; Millet, O.; Labeikovsky, W.; Korzhnev, D. M.; Wolf-Watz, M.; Bosco, D. A.; Skalicky, J. J.; Kay, L. E.; Kern, D. *Nature* **2005**, *438*, 117−121.
(12) Rasmussen, S. G. F.; Choi, H.-J.; Fung, J. J.; Pardon, E.; Casarosa, P.; Chae, P. S.; DeVree, B. T.; Rosenbaum, D. M.; Thian, F. S.; Kobilka, T. S.; Schnapp, A.; Konetzki, I.; Sunahara, R. K.; Gellman, S. H.; Pautsch, A.; Steyaert, J.; Weis, W. I.; Kobilka, B. K. *Nature* **2011**, *469*, 175−180.
(13) Steyaert, J.; Kobilka, B. K. *Curr. Opin. Struct. Biol.* **2011**, *21*, 567−572.
(14) Lipari, G.; Szabo, A. *J. Am. Chem. Soc.* **1982**, *104*, 4546−4559.
(15) Lipari, G.; Szabo, A. *J. Am. Chem. Soc.* **1982**, *104*, 4559−4570.
(16) Rasmussen, S. G. F.; DeVree, B. T.; Zou, Y.; Kruse, A. C.; Chung, K. Y.; Kobilka, T. S.; Thian, F. S.; Chae, P. S.; Pardon, E.; Calinski, D.; Mathiesen, J. M.; Shah, S. T. A.; Lyons, J. A.; Caffrey, M.; Gellman, S. H.; Steyaert, J.; Skiniotis, G.; Weis, W. I.; Sunahara, R. K.; Kobilka, B. K. *Nature* **2011**, *477*, 549−555.
(17) Sykes, B. D.; Weingarten, H. I.; Schlesinger, M. J. *Proc. Natl. Acad. Sci. U.S.A.* **1974**, *71*, 469−473.
(18) Yao, X.; Parnot, C.; Deupi, X.; Ratnala, V. R. P.; Swaminath, G.; Farrens, D.; Kobilka, B. *Nat. Chem. Biol.* **2006**, *2*, 417−422.
(19) Liu, J. J.; Horst, R.; Katritch, V.; Stevens, R. C.; Wüthrich, K. *Science* **2012**, *335*, 1106−1110.
(20) Chung, K. Y.; Kim, T. H.; Manglik, A.; Alvares, R.; Kobilka, B. K.; Prosser, R. S. *J. Biol. Chem.* **2012**, *287*, 36305−36311.
(21) Yao, X. J.; Velez-Ruiz, G.; Whorton, M. R.; Rasmussen, S. G. F.; DeVree, B. T.; Deupi, X.; Sunahara, R. K.; Kobilka, B. *Proc. Natl. Acad. Sci. U.S.A.* **2009**, *106*, 9501−9506.
(22) Palmer, A. G., III. *Chem. Rev.* **2004**, *104*, 3623−3640.
(23) Kay, L. E. *J. Magn. Reson.* **2005**, *173*, 193−207.
(24) Cavanagh, J.; Fairbrother, W. J.; Palmer, A. G., III; Rance, M.; Skelton, N. J. *Protein NMR Spectroscopy: Principles and Practice*, 2nd ed.; Academic Press: Burlington, MA, 2007.
(25) Tanner, J. E. *J. Chem. Phys.* **1970**, *52*, 2523.

(26) Kitevski-LeBlanc, J. L.; Prosser, R. S. *Prog. Nucl. Magn. Reson. Spectrosc.* **2012**, *62*, 1−33.
(27) Ghanouni, P.; Gryczynski, Z.; Steenhuis, J. J.; Lee, T. W.; Farrens, D. L.; Lakowicz, J. R.; Kobilka, B. K. *J. Biol. Chem.* **2001**, *276*, 24433−24436.
(28) Kofuku, Y.; Ueda, T.; Okude, J.; Shiraishi, Y.; Kondo, K.; Maeda, M.; Tsujishita, H.; Shimada, I. *Nat. Commun.* **2012**, *3*, 1045.
(29) Nygaard, R.; Zou, Y.; Dror, R. O.; Mildorf, T. J.; Arlow, D. H.; Manglik, A.; Pan, A. C.; Liu, C. W.; Fung, J. J.; Bokoch, M. P.; Thian, F. S.; Kobilka, T. S.; Shaw, D. E.; Mueller, L.; Prosser, R. S.; Kobilka, B. K. *Cell* **2013**, *152*, 532−542.
(30) Orban, T.; Jastrzebska, B.; Gupta, S.; Wang, B.; Miyagi, M.; Chance, M. R.; Palczewski, K. *Structure* **2012**, *20*, 826−840.
(31) Kobilka, B. K. *Trends. Pharmacol. Sci.* **2011**, *32*, 213−218.
(32) Koshland, D. E. *Angew. Chem., Int. Ed. Engl.* **1995**, *33*, 2375−2378.
(33) Imai, H.; Mizukami, T.; Imamoto, Y.; Shichida, Y. *Biochemistry* **1994**, *33*, 14351−14358.
(34) Choe, H.-W.; Park, J. H.; Kim, Y. J.; Ernst, O. P. *Neuropharmacology* **2011**, *60*, 52−57.
(35) Hofmann, K. P.; Scheerer, P.; Hildebrand, P. W.; Choe, H.-W.; Park, J. H.; Heck, M.; Ernst, O. P. *Trends Biochem. Sci.* **2009**, *34*, 540−552.
(36) Dror, R. O.; Arlow, D. H.; Borhani, D. W.; Jensen, M. O.; Piana, S.; Shaw, D. E. *Proc. Natl. Acad. Sci. U.S.A.* **2009**, *106*, 4689−4694.
(37) Moukhametzianov, R.; Warne, T.; Edwards, P. C.; Serrano-Vega, M. J.; Leslie, A. G. W.; Tate, C. G.; Schertler, G. F. X. *Proc. Natl. Acad. Sci. U.S.A.* **2011**, *108*, 8228−8232.
(38) Popovych, N.; Sun, S.; Ebright, R. H.; Kalodimos, C. G. *Nat. Struct. Mol. Biol.* **2006**, *13*, 831−838.
(39) Boehr, D. D.; Nussinov, R.; Wright, P. E. *Nat. Chem. Biol.* **2009**, *5*, 789−796.
(40) Liu, W.; Chun, E.; Thompson, A. A.; Chubukov, P.; Xu, F.; Katritch, V.; Han, G. W.; Roth, C. B.; Heitman, L. H.; Ijzerman, A. P.; Cherezov, V.; Stevens, R. C. *Science* **2012**, *337*, 232−236.
(41) Angel, T. E.; Chance, M. R.; Palczewski, K. *Proc. Natl. Acad. Sci. U.S.A.* **2009**, *106*, 8555−8560.
(42) Angel, T. E.; Gupta, S.; Jastrzebska, B.; Palczewski, K.; Chance, M. R. *Proc. Natl. Acad. Sci. U.S.A.* **2009**, *106*, 14367−14372.
(43) Seifert, R.; Wenzel-Seifert, K.; Gether, U.; Lam, V. T.; Kobilka, B. K. *Eur. J. Biochem.* **1999**, *260*, 661−666.
(44) Westfield, G. H.; Rasmussen, S. G. F.; Su, M.; Dutta, S.; DeVree, B. T.; Chung, K. Y.; Calinski, D.; Velez-Ruiz, G.; Oleskie, A. N.; Pardon, E.; Chae, P. S.; Liu, T.; Li, S.; Woods, V. L.; Steyaert, J.; Kobilka, B. K.; Sunahara, R. K.; Skiniotis, G. *Proc. Natl. Acad. Sci. U.S.A.* **2011**, *108*, 16086−16091.